Proton emission in inelastic scattering of ^{40}Ca on ^{40}Ca at 50 MeV/nucleon

J. A. Scarpaci,[1] M. Lamehi-Rachti,[1,*] J. C. Roynette,[1] Y. Blumenfeld,[1] Ph. Chomaz,[2] N. Frascaria,[1] J. P. Garron,[1] T. Suomijärvi,[1] D. Beaumel,[1] I. Lhenry,[1] N. Alamanos,[3] A. Gillibert,[3] and A. van der Woude[4]

[1]*Institut de Physique Nucléaire, IN$_2$P$_3$-CNRS, 91406 Orsay, France*

[2]*GANIL/CEA/DSM, CNRS(IN2P3), BP 5027, 14076 Caen Cedex 5, France*

[3]*CEA/DSM/DAPNIA/SPhN Saclay, 91191 Gif sur Yvette Cedex, France*

[4]*Kernfysisch Versneller Institut, 9747 AA Groningen, The Netherlands*

(Received 26 March 1997)

Inelastic scattering of ^{40}Ca on ^{40}Ca at 50 MeV/nucleon has been measured in coincidence with light charged particles detected over a large angular domain. The giant resonance region of the inelastic spectrum is shown to be dominated by the isoscalar giant quadrupole resonance. The characteristics of the emitted protons allow us to separate four reaction mechanisms contributing to the high excitation energy region of the inelastic spectrum ($E^* > 30$ MeV): pickup breakup, knockout, inelastic scattering to high-lying target states, and a new mechanism responsible for the emission of fast-moving protons. A sizable direct decay branch towards hole states of ^{39}K is measured for the giant quadrupole resonance in ^{40}Ca. Evidence is given for the excitation of the two-phonon giant quadrupole resonance, characterized by its direct decay scheme. The energy and width of this two-phonon state are in agreement with a harmonic picture for collective nuclear excitations. [S0556-2813(97)03612-1]

PACS number(s): 24.30.Cz, 24.50.+g, 25.70.Bc

I. INTRODUCTION

In the late 1970s, the study of dissipative heavy-ion collisions revealed intriguing effects in the energy spectra of inelastically scattered nuclei in heavy-ion collisions. A detailed examination of the inelastic channel, showed the existence of small regularly spaced structures in the incompletely relaxed region of the energy spectra, superimposed on a large background. These structures were first observed in the ^{40}Ca+^{40}Ca and ^{63}Cu+^{63}Cu collisions at low incident energies (7 and 10 MeV per nucleon) [1,2]. Their main characteristics are their regular spacing, their relatively narrow widths, and their angular distributions strongly peaked around the grazing angle. A semiclassical calculation was developed [3], based on a microscopic description of the giant resonances (GRs) excited while the heavy ions travel on classical trajectories, which predicted the excitation of multiphonon states. Thereafter, a tentative interpretation of the observed bumps in terms of multiphonon states built with GRs was given.

The onset of new accelerators delivering heavy ions at intermediate energies (30 to 100 MeV per nucleon) stimulated new research in this field. A large number of inelastic scattering experiments were performed at GANIL, with various projectile-target combinations at different incident energies around 50 MeV/nucleon [4,5]. The great improvement in energy resolution obtained with the use of a magnetic spectrometer led to a quantitative understanding of the GRs excited in these reactions with very large differential cross sections and peak to background ratios [6,7], offering favorable conditions for the observation of multiphonon states.

However, progress in the understanding of higher lying structures was hampered by the fact that many mechanisms, besides the excitation of the target, contribute to the inelastic excitation spectrum. In order to disentangle the target excitation from the different reaction mechanisms occurring in the inelastic channel, coincidence experiments between scattered projectile and light particles are necessary. Indeed, light particles stemming from the decay of collective modes excited in the slowly recoiling target nucleus are emitted in all directions in the laboratory frame, whereas reaction mechanisms known to populate the inelastic channel such as pickup breakup [8] or knockout, give rise to very specific angular distributions of the emitted particles, focused around the direction of the ejectile in the former case and around the direction of the recoiling target in the latter. Coincidence experiments not only allow us to identify the different reaction mechanisms and to unambiguously select target excitations in the inelastic spectra, but they also might provide a signature for multiphonon states by the study of their decay.

In this paper, we will report on the results concerning the inelastic scattering of 50 MeV/nucleon ^{40}Ca on ^{40}Ca target studied in coincidence with light charged particles. This system has been chosen for many reasons. First of all, properties of giant resonances in ^{40}Ca are well documented from numerous previous experiments [9]. The ^{40}Ca+^{40}Ca reaction has been extensively studied previously in inclusive experiments at different lower incident energies. At about 50 MeV/nucleon, and for intermediate mass nuclei such as ^{40}Ca, calculations show that the nuclear interaction is predominant and will excite mainly isoscalar GRs; the contribution of the isovector giant dipole resonance is expected to be relatively small. Moreover, at this bombarding energy the particles emitted by the projectilelike and the targetlike sources are well separated in velocity space allowing to disentangle the contribution of the target excitation from the other mechanisms.

In the following, an extensive analysis of the inelastic channel from the ^{40}Ca+^{40}Ca reaction will be presented. Af-

*On leave from University of Teheran, Iran.

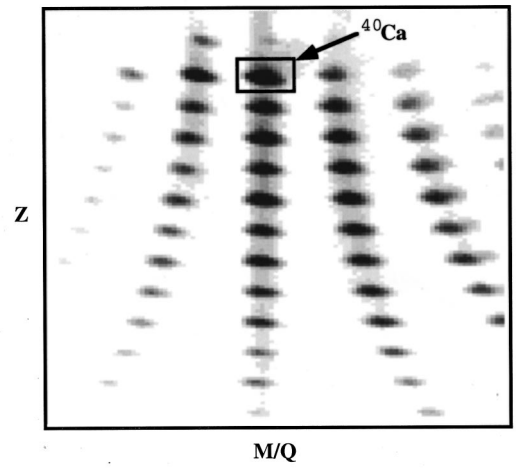

FIG. 1. Mass and charge identification of the ejectiles. The M/Q parameter is related to the time of flight of the ejectile and the Z parameter to the energy loss in the ionization chamber.

ter the description of the experimental set up in Sec II, inclusive data will be presented and the multipole composition of the giant resonance bump observed in ^{40}Ca will be analyzed in Sec. III. The different mechanisms contributing to the inelastic spectrum will be extracted from the coincidence data and discussed in Sec. IV. Section V will be devoted to the study of the decay of the GR and the multiphonon states, and a new method to sign the presence of multiphonon strength in the inelastic spectrum will be emphasized. Conclusions will be drawn in Sec. VI. Some of the results presented in this paper have previously been published [10,11]. Comprehensive reviews on the subject of multiphonon excitations can be found in [12,13].

II. EXPERIMENTAL METHOD

The experiment was performed at the GANIL facility, by bombarding an evaporated self-supported 0.5 mg/cm^2 ^{nat}Ca target with a 50 MeV/nucleon ^{40}Ca beam.

A. Detection of the scattered fragments

The inelastically scattered fragments were measured between $\theta_{lab}=1°$ and 5° (the grazing angle for this reaction is approximately 1°) using the SPEG spectrometer with its standard detection system [14]: two drift chambers for position measurements and an ionization chamber backed by a plastic scintillator for particle identification. The ionization chamber gives a measurement of the atomic number Z of the detected fragment while a time of flight measurement with a resolution of 500 ps, obtained between the plastic signal and the RF of the cyclotron, allows to separate the different mass over charge ratios A/Q. Unambiguous identification of $^{40}Ca^{20+}$ was obtained as shown in Fig. 1. An excitation energy range of about 150 MeV was covered in one setting of the magnetic field. The measured total energy resolution was 800 keV. The angular resolution was approximately 0.2°.

B. Light particle detection

Light charged particles were detected in 29 cesium iodide (CsI) elements of the multidetector array PACHA [15].

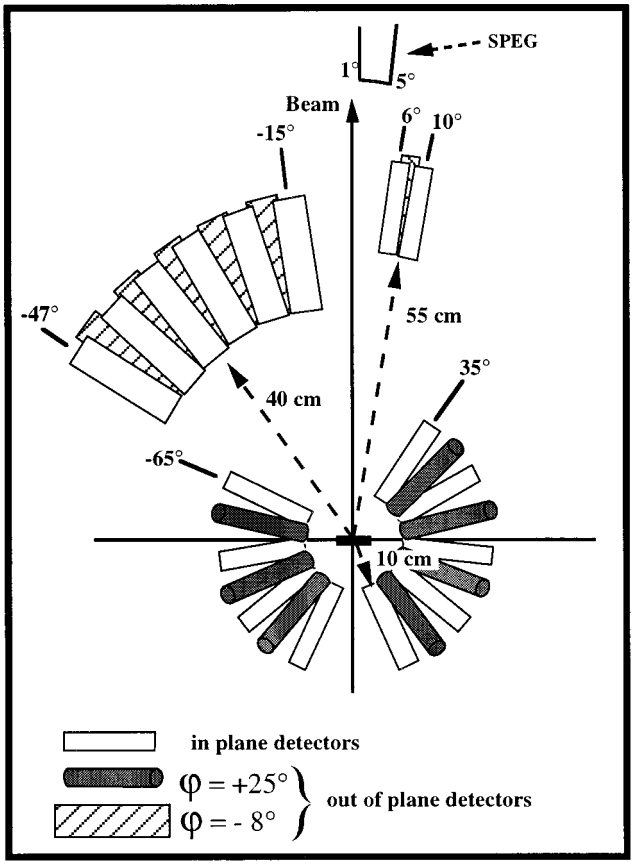

FIG. 2. Experimental setup indicating the positions of the CsI detectors. SPEG indicates the in-plane angular acceptance of the spectrometer. See text for more details.

These detectors consist of cylindrical CsI crystals of 30 mm thickness available in two diameters: 15 and 33 mm. Permanent magnets are placed in front of all the detectors to shield the detectors from secondary electrons coming from the target. The crystals are read out by photomultipliers. On each detector, an optical fiber connected to a light emitting diode allows to check the system operation and the gain stability during the experiment.

Figure 2 shows the position of the detectors around the target. The system covered the whole angular domain with the exception of small wedges between $-15°$ and $+6°$ around the beam direction and between $+10°$ and $+35°$. Positive angles refer to the same side of the beam as the spectrometer. The detectors can be separated into three groups. From $+35°$ to $-65°$ (clockwise), sixteen small detectors are positioned 10 cm away from the target. Nine are in the horizontal plane located every 15°, and seven are placed in between these detectors, 25° out of plane. In the forward direction, on the left side of the beam, eleven 33 mm diameter detectors set at 40 cm from the target cover the angular range between $-47°$ and $-15°$, five are in the horizontal plane and six are located 8° out of plane. On the right side of the beam, three small detectors are set at 55 cm from the target, close to beam direction at $+6°$, $+8°$ and $+10°$. The total solid angle covered by the CsI detectors is 3% of 4 π.

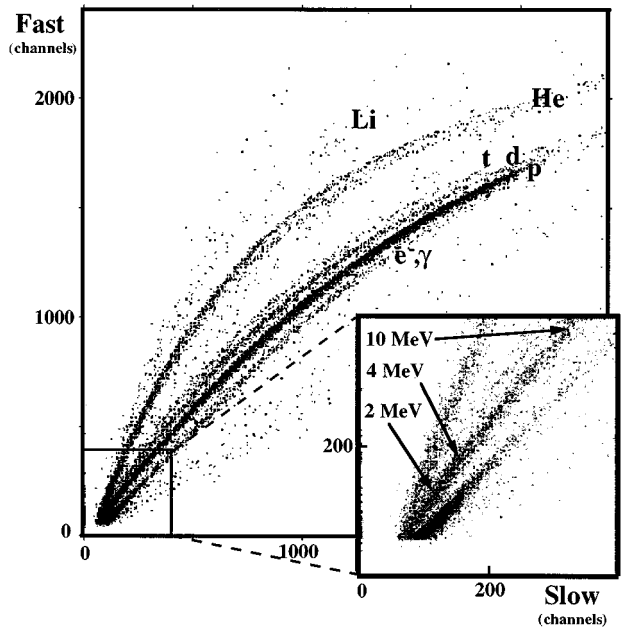

FIG. 3. Particle identification with the cesium iodide detectors of the Pacha ensemble. The fast component is the result of the integration of the photomultiplier output signal in a 400 ns gate while the slow component results from the integration in a gate 1.5 μs wide beginning 1.6 μs after the start of the signal. The inset is a zoom of the low energy part of the figure. Arrows indicate the calibration for protons.

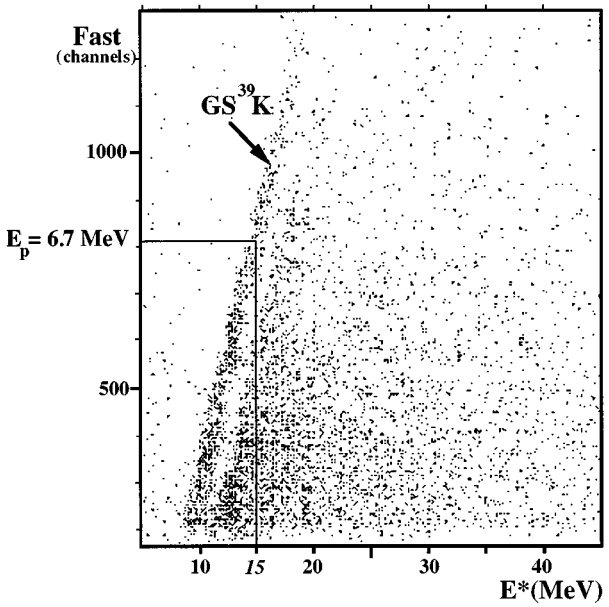

FIG. 4. Excitation energy of the system versus the fast component of a CsI detector for coincidence events between a ^{40}Ca ejectile and a proton. One can observe a well separated line corresponding to events where protons are feeding the ground state of the daughter nucleus ^{39}K. These two-dimensional plots allow to calibrate the CsI detectors for protons. An example of correspondence between excitation energy and proton kinetic energy is shown.

Protons, deuterons, tritons, and α particles were identified by pulse shape analysis. A ''fast'' component was obtained by integrating the signal in a 400 ns wide gate and a ''slow'' component was given by the integration in a 1.5 μs wide gate, starting 1.2 μs after the end of the fast gate. A typical fast versus slow bidimensional plot is displayed in Fig. 3 and shows the unambiguous identification of the proton and α particles down to 2 and 5 MeV, respectively. At lower energies, a time of flight measurement between CsI detectors and the cyclotron RF allows to unambiguously identify the different particles.

The light particle energy calibrations were performed by detecting momentum analyzed secondary light particle beams in all the counters set at zero degrees. However the production of a proton beam of less than 10 MeV could not be achieved. For lower energies, the particle decay towards the ground state (GS) of the daughter nucleus provided an excellent energy calibration. This is demonstrated in Fig. 4 which shows for an inelastically scattered ejectile in coincidence with a proton the reconstructed excitation energy of the target versus the fast component of the CsI. In this two dimensional plot, discrete levels of the daughter nucleus appear as tilted lines. As the initial target excitation energy is known from two-body kinematics, the GS line yields a direct calibration of the fast component into proton kinetic energy.

The energy resolution for protons was close to 2% above 20 MeV, dropping to about 6% around 10 MeV. The detection threshold ranged between 1 and 3.5 MeV for protons and approximately 5 MeV for α particles depending on the counter. In order to be able to add the data from various detectors, a software threshold of 4 MeV for protons in the center of mass of the recoiling ^{40}Ca nucleus was used during the analysis.

III. INCLUSIVE DATA

Figure 5 displays the inclusive inelastic spectrum for $1.7° \leqslant \theta_{\rm lab} \leqslant 5°$. Inclusive inelastic data for angles below $\theta = 1.7°$ could not be used because of the presence of the scattering from the hydrogen contamination in the target. In

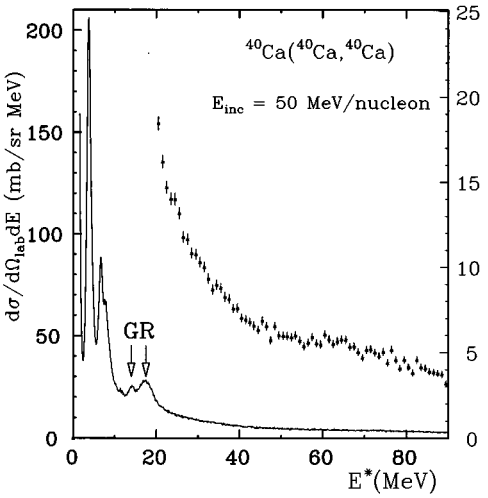

FIG. 5. Inclusive inelastic spectrum with 100 keV/channel energy binning (bottom) and 1 MeV/channel energy binning (top). Left-hand scale refers to lower spectrum and right-hand scale to upper spectrum.

TABLE I. Parameters for the optical potential.

V (MeV)	r_v (fm)	a_v (fm)	W (MeV)	r_w (fm)	a_w (fm)	r_c (fm)
20.1	1.28	0.67	14.8	1.28	0.67	1.2

the lower excitation region, the spectrum exhibits several discrete peaks. The state located at 3.74 MeV corresponds to the well-known first collective 3^- state in ^{40}Ca which can be excited both in the projectile and the target nuclei since it is located below the particle emission threshold. A group of states is observed at around 7 MeV excitation energy. At higher excitation energy, the large bump of the GR dominates the spectrum with a peak-to-background ratio close to one. It is split into two components centered at 14 and 17.5 MeV excitation energy. It was observed that the relative intensities of the two components of the GR integrated over different angular domains remain the same, suggesting that only one L-multipolarity component dominates. When the energy scale is compressed (1 MeV/channel), some small bumps are observed at energies above the GR. In this region, calculations [16] predict that the strongest resonant contribution comes from multiphonon states built with the GR. A weaker but sizable contribution from high multipolarity one-phonon GRs (mainly $L=3$ and $L=4$) is also expected. The isovector GQR is predicted to be located in the same region, however, its cross section should be very low due to the relatively weak contribution of the Coulomb interaction in the reaction studied. Around 60 MeV excitation energy, a large plateau is observed in the inelastic spectrum due to three-body processes such as pickup breakup. This mechanism will be discussed later in the paper.

In order to analyze the data, inelastic angular distributions were calculated using the coupled channel code ECIS [17] and standard collective form factors. The optical model potentials were obtained by fitting the measured elastic scattering angular distributions. The set of parameters used is listed in Table I. The validity of these parameters has been checked by applying them to the angular distribution calculation of the collective 3^- level. Although this level at 3.74 MeV cannot be separated from the 2^+ level at 3.90 MeV, the cross section of the 3^- state is expected to be ten times larger than for the 2^+ state when using the sum-rule values obtained in Ref. [18].

The experimental angular distribution of the peak at 3.7 MeV is displayed on Fig. 6 and shows an excellent agreement with the calculation for an $L=3$ transition. Taking into account that the state can be excited in both the projectile and the target, a $B(E3)$ value of 9.3 W.u. is extracted. This value is lower than the adopted values of 30.7 W.u. reported in the literature [19]. Similarly low $B(E3)$ values have been systematically extracted from heavy-ion collisions as reported by Ref. [7]. According to Ref. [20], this apparent hindrance of the 3^- excitations induced by nuclear scattering is a consequence of the use of the deformed optical potential model for the analysis of hadronic scattering. This discrepancy disappears when a folding model analysis is used.

The theoretical angular distribution of the isoscalar $L=0$, 2–6 resonances and of the $L=1$ isovector resonance, calculated at 17 MeV excitation energy and for 100% of the energy weighted sum rule (EWSR), are shown on Fig. 7. For

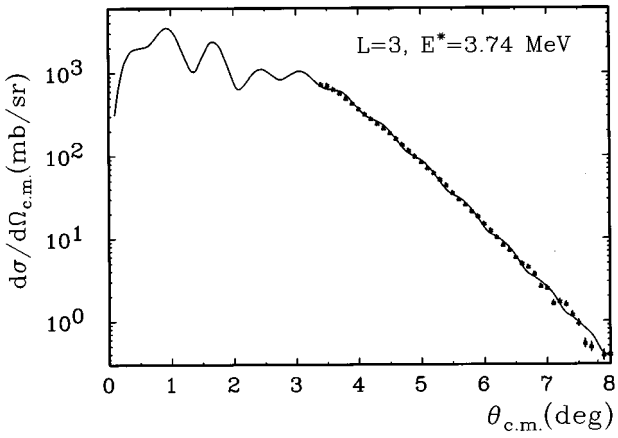

FIG. 6. Angular distribution of the 3.7 MeV peak. Solid line represents the DWBA ECIS calculation performed as described in text.

multipolarities $L \geq 3$ the angular distributions are not characteristic of the multipolarity. This feature is a well-known drawback of the use of heavy-ion beams for the study of GRs, compared to light hadronic probes [6]. The $L=0$ and $L=2$ distributions can only be distinguished from the other isoscalar distributions at very small angles. The isovector $L=1$ resonance, which is only excited by the Coulomb interaction, presents a very distinct distribution with a strong maximum near the grazing angle and a steeper slope at large angles compared to the isoscalar resonances. However, in the present experiment, the Coulomb interaction is relatively weak and in the angular range $3.4° \leq \theta_{\text{c.m.}} \leq 10°$, the cross section for the isovector giant dipole resonance is expected to be small.

A general method for heavy ion scattering to extract the different multipolarities contributing to the giant resonance peak was described in Ref. [21]. In this procedure the inelastic spectrum is divided into small energy bins and the angu-

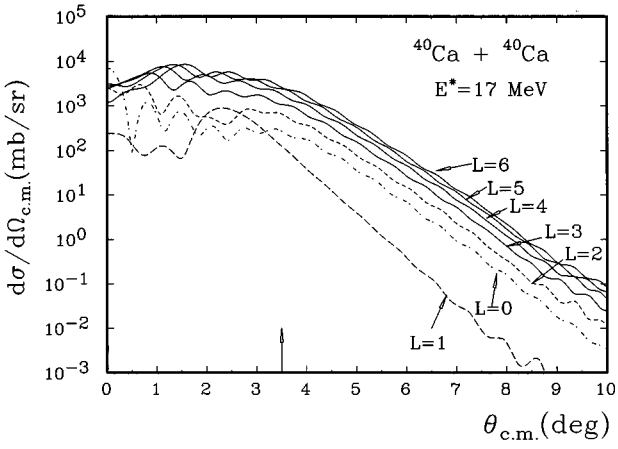

FIG. 7. Theoretical angular distributions of the isoscalar $L=0$,2-6 resonances and of the $L=1$ isovector resonance, calculated with the DWBA code ECIS at 17 MeV excitation energy and for 100% of the energy weighted sum rule (EWSR). The arrow indicates the smallest angle for which the inclusive data could be analyzed.

lar distribution is extracted for each bin. The angular distribution is then fitted using a minimum-χ^2 procedure by a linear combination of the theoretical angular distributions calculated for different multipolarities and possibly a background angular distribution.

$$\frac{d\sigma_{\rm exp}}{d\Omega}(E)=\sum_L S_L(E)\frac{d\sigma_L}{d\Omega}(E)+\frac{d\sigma_B}{d\Omega}(E),$$

where $(d\sigma_{\rm exp}/d\Omega)(E)$ is the experimental differential cross section for the energy bin centered at E, $(d\sigma_L/d\Omega)(E)$ is the calculated differential cross section for 100% of the energy weighted sum rule (EWSR), $S_L(E)$ is the percentage of the sum rule exhausted by the L component in the E energy bin and $(d\sigma_B/d\Omega)(E)$ the background angular distribution.

This method relies on the sensitivity of the angular distributions to the multipolarity. In the present case, the calculations described above show that the method will only allow to separate the cross section into three components: the isoscalar resonances $L=0$ and $L\geqslant 2$, the isovector $L=1$ resonance and the background. The isovector dipole resonance is expected to contribute very weakly to the resonance bump in the angular range considered, and the method is not sensitive enough to allow a precise extraction of its cross section. Therefore, the isovector dipole contribution was calculated assuming a Lorentzian shape with a mean energy of 20 MeV, a width of 5.5 MeV, and exhausting 100% of the Thomas-Reiche-Kuhn sum rule. The exponential dependence of the Coulomb excitation probability, which results in an enhancement of the low-energy portion of the resonance and to an average shift of its centroid [6] was taken into account. After subtraction of this $L=1$ component, the inelastic spectrum was divided into 1 MeV bins and the angular distribution of each bin was extracted. Each angular distribution was then fitted by a linear combination of the calculated angular distribution for $L=2$ and the angular distribution of the background which was assumed to be similar to the angular distribution of the energy region located immediately above the GRs. An example of the fit is shown in Fig. 8 for the region between 15 and 16 MeV excitation energy. Both the $L=2$ and the background angular distributions are shown as well as their sum. Similar quality fits were obtained for all the energy bins.

The final result of the decomposition is represented in Fig. 9. As mentioned above, in the angular range studied in this analysis (from 1.7° to 5° in the laboratory), the $L=1$ component has a negligible contribution to the cross section as shown in the figure. The background component extracted from this analysis is approximately constant over all the excitation energy range. The main part of the cross section can be attributed to $L=0$ or $L\geqslant 2$ multipolarities which exhibit two components. Assuming only $L=2$, the EWSR sum rule is about 40 ± 10 % in the 12 to 22 MeV excitation energy region, compatible with the results reported in the literature [9], although it is slightly smaller than the mean value of these results. It should be noted that any small contribution of higher multipolarity would strongly decrease this value. In the following, only $L=2$ strength will be assumed. Note that the use of the deformed potential model may slightly decrease the extracted sum rule strength compared to a complete folding model analysis. This effect increases with higher multipolarities but has been shown to be significant even for $L=2$ in the case of light nuclei [20].

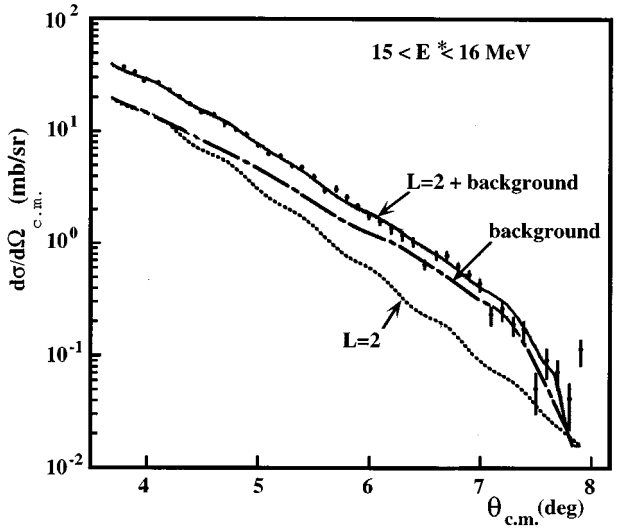

FIG. 8. Fit of the experimental angular distribution (dots) by a linear combination of the calculated angular distribution for $L=2$ (dotted line) and the angular distribution of the background (dash dotted line), for the region between 15 and 16 MeV excitation energy.

IV. COINCIDENCE DATA-REACTION MECHANISMS

In the following, we will show the potential of the coincidence measurement to disentangle the mechanisms contributing to the inelastic channel. In the present experiment only proton coincidence data will be discussed. Figure 10 shows a density plot of the invariant cross section for protons in the $(V_\parallel, V_\perp)$ velocity plane, corrected for detector solid angles, in coincidence with the inelastic channel, i.e., a ^{40}Ca detected in the spectrometer. In this plot, no gate is placed on the energy of the ^{40}Ca. Random coincidences, which contributed less than 10% of the total counting rate, were sub-

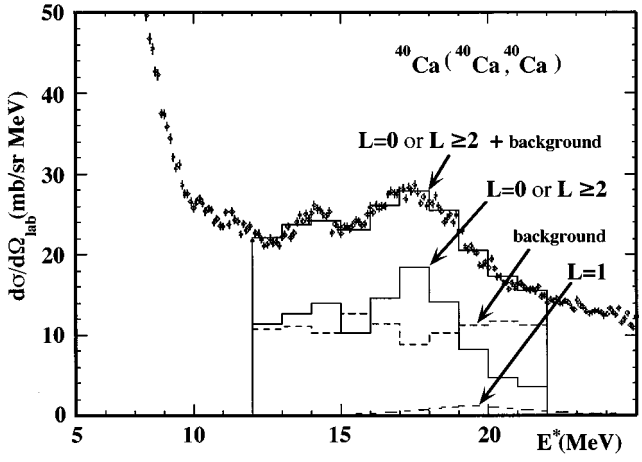

FIG. 9. Decomposition of the GR region into $L=0$ or $L\geqslant 2$ multipolarities and the background. The $L=1$ component is also represented for 100% of the EWSR.

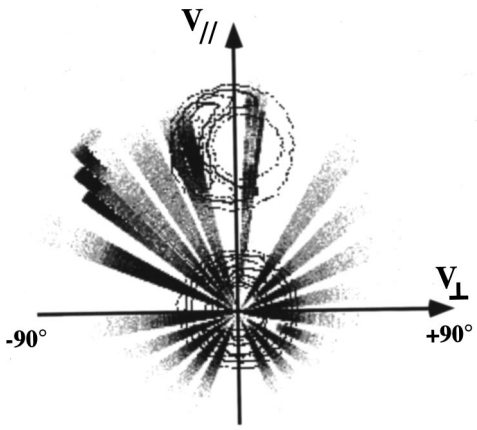

FIG. 10. Experimental invariant proton cross section represented in the $(V_{\parallel},V_{\perp})$ plane in coincidence with inelastic scattering. Each cone corresponds to one proton detector. The arrow indicates the average velocity of the ^{40}Ca ejectile detected in the spectrometer on the right side of the beam. Contour plot: Monte Carlo simulation of the invariant proton cross section in coincidence with inelastic scattering for the pickup breakup and the target decay (see text).

tracted. In the forward direction around $\theta_p=-15°$ and $+8°$, an accumulation of fast moving protons is observed which is characteristic of the presence of the pickup breakup mechanism. An almost isotropic component of low velocity protons centered around the recoiling target nucleus reflects the decay of states excited in the target through inelastic scattering. At negative angles, around $-50°$, the proton yield is strongly enhanced by recoiling protons stemming from the elastic scattering on the hydrogen contaminant of the target. The knockout process onto protons from the target is also expected to give rise to protons around this recoiling angle. Another interesting feature is apparent around $+40°$ where fast protons (up to 50 MeV kinetic energy) are present, which are not observed at the most backward angles. This component cannot be accounted for by the decay of the projectile or the target and will be discussed in Sec. IV C. In the backward hemisphere in the laboratory frame, only protons coming from the decay of the target are emitted. Therefore, the measurement of inelastic scattering in coincidence with backward emitted protons is a method to focus on pure inelastic scattering by eliminating the other mechanisms which give rise to particles emitted in the forward direction.

A. The pick-up break-up process

Pickup breakup reactions (PUBU) occur when the projectilelike fragment produced in a one-nucleon pick-up reaction decays in flight by re-emitting the captured nucleon [8]. The secondary light particles are assumed to be emitted isotropically in the projectilelike fragment frame, thus, their laboratory velocity is boosted by the velocity of the projectilelike fragment. At 50 MeV/nucleon incident energy, they are well separated from the particles emitted by the decay of the target (see Fig. 10). Measurements of the velocity of the light particles emitted in coincidence with the ejectiles is thus a very efficient tool to discriminate the pickup breakup reactions from the target excitations. In the present experiment the main pickup breakup contribution comes from the following reaction:

$$^{40}\mathrm{Ca}+^{40}\mathrm{Ca}\rightarrow{}^{41}\mathrm{Sc}+{}^{39}\mathrm{K}$$
$$\downarrow$$
$$^{40}\mathrm{Ca}+p.$$

Note that in simple transfer reactions at intermediate energies it has been shown that the donor nucleus (in this case the targetlike nucleus) is very weakly excited [22,23], and thus the major part of the excitation energy of the system can be attributed to the projectilelike fragment.

A Monte Carlo simulation has been performed for the PUBU mechanism. In this calculation only the one-proton pickup channel was taken into account. The excitation energy distribution of the ^{41}Sc was chosen as a Gaussian centered at 15 MeV, with a variance of 7 MeV, to favor single proton emission by the quasiprojectile. For higher excitation energies the ^{41}Sc will emit more than one light particle, and the daughter nucleus will not populate the inelastic channel. The shape of the excitation energy distribution was found not to affect the final result. The decay of the excited nuclei was calculated using a modified version [24] of the Monte Carlo evaporation code LILITA [25] which calculates the kinetic energy of emitted light particles on an event by event basis. The characteristic proton ring shown in Fig. 10 as a contour plot, corresponding to the emission from the projectilelike fragment, is concentrated in a cone of approximately 30° opening angle in the laboratory frame. Note that the asymmetry of the projectile ring observed in the calculation arises from a kinematical effect due to the forward focused primary angular distribution of the transfer products [26].

The inelastic scattering, leading to the excitation of the target, has also been simulated. The emitted protons coming from the target present an almost isotropic component in the laboratory frame, nicely reproducing the ring centered around the recoiling target.

Figure 11 shows the ^{40}Ca spectra in coincidence with protons detected at $\theta_p=+8°$ [Fig. 11(a)] and $-15°$ [Fig. 11(b)], where the pickup breakup process is prevalent. The two spectra exhibit very different shapes, due to the fact that two kinematical solutions (forward and backward) are allowed for proton emission at the angle closest to the ejectile ($\theta_p=+8°$), while at an angle further away ($\theta_p=-16°$), corresponding to the edge of the proton ring, these two solutions are degenerate (see Fig. 10). The Monte Carlo calculation (represented by histograms) gives a very good description of the data, using only one overall normalization coefficient for the two spectra. The relative normalization depends mainly upon the angular distribution of the primary transfer products, which was chosen to be equal to the experimental ^{41}Sc distribution. Note that the calculation was performed assuming no excitation of the target nucleus. An excitation energy E_t^* in the target would shift the spectra towards higher apparent excitation energies by a quantity equal to E_t^* [8]. The agreement obtained confirms that during the transfer process, the donor nucleus (here the target) is at most weakly excited.

Applying the normalization factor, previously found to fit

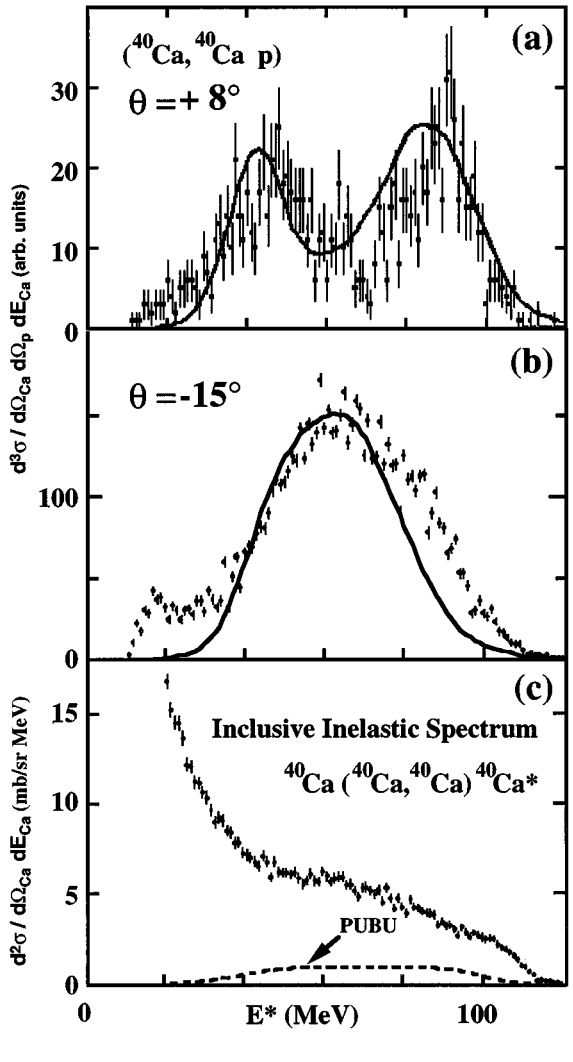

FIG. 11. Inelastic spectra in coincidence with protons detected at $\theta_p = +8°$ (a) and $-16°$ (b), where the pickup breakup process is prevalent. The LILITA Monte Carlo calculation is represented by solid lines. (c) Contribution of the proton pickup breakup process to the inclusive inelastic spectrum.

the coincidence data, to the full calculation without any constraint on the proton angle allows to estimate the total contribution of the pickup breakup process to the inclusive inelastic cross section. The result displayed by a histogram is compared to the inclusive experimental spectrum in Fig. 11(c). The proton pickup breakup reaction accounts for only about 20% of the inelastic cross section in the region between 50 and 90 MeV excitation energy. Since neutrons were not detected in this experiment, the neutron pickup breakup contribution can only be grossly estimated by theoretical considerations. Distorted-wave Born approximation (DWBA) calculations using the code PTOLEMY [27] predict that, for an excitation energy of the projectilelike fragment of 15 MeV, proton transfer is about twice as probable as neutron transfer, which can be explained by the large neutron binding energy in ^{40}Ca. Moreover, the statistical decay code CASCADE [28] shows that a ^{41}Sc nucleus excited to 15 MeV will decay with 60% probability by single proton emission, while a ^{41}Ca, produced by neutron transfer, with the same excitation energy, has only a 25% probability of deexciting by single neutron emission. Combining the formation and decay probabilities, the neutron pickup breakup cross section is expected to be about one quarter of the proton pickup breakup cross section in the reaction studied. Even making allowance for a large uncertainty in this prediction, the pickup breakup mechanism cannot account for more than 30% of the total cross section in the high excitation energy region of the inelastic spectrum. It should be noted that this value strongly depends on the reaction studied since the transfer probabilities are expected to depend dramatically upon projectile-target combination and bombarding energy [29].

Apart from the pickup breakup contribution, three other proton components are present; protons arising from the decay of excited target states, a possible knockout of nucleons of the target by the projectile and fast protons focused at angles on the same side of the beam as the ejectile arising from a new mechanism that will be discussed in the following. To disentangle these three components, the proton angular correlations will now be investigated.

B. Angular correlations

From a theoretical point of view, the calculation of the angular correlation functions for the decay of an excited nucleus, implies the knowledge of the two main steps of the reaction. The first step is the excitation of the target through the inelastic reaction, usually described in the framework of DWBA calculations. The second step is the subsequent decay of the excited state.

The probability distribution $W_L(\theta,\phi)$ which governs the angular correlation of light particles depends on the quantum numbers $(J_i^\pi, m_i, J_f^\pi, m_f)$, of the intermediate and the final state, respectively, and it depends also on the characteristics of the decay channel: spin (s_p), energy (E_p), and angular momentum (l) of the emitted particle. A full calculation of the probability distribution would require the knowledge of both the population of the magnetic substates for the intermediate state and the details of the wave function for the emitted particle. The angular correlation function takes a simple form in the plane wave Born approximation for a pure L intermediate state decaying via a spinless particle (α particle) toward a $J^\pi = 0^+$ final state. The quantization axis is taken along the recoil axis, so that only the $m=0$ magnetic substate is populated. In this case the correlation function can be expressed as a function of spherical harmonics [30]. The correlation function exhibits a symmetric pattern around $\pm 90°$ in the rest frame of the recoil nucleus and the shape of the experimental correlation gives a direct access to the spin of the intermediate state. In the present experiment, where the emitted particle is a proton, several l values can be involved in the decay channel and the extraction of the intermediate state characteristics is no longer straightforward. Finally, the probability that several intermediate states can contribute is high and this effect should also be taken into account. Consequently, in the present paper, we will limit ourselves to a qualitative discussion of the experimental angular correlations.

Figure 12 displays the angular distributions of protons emitted in coincidence with ^{40}Ca fragments detected in the SPEG spectrometer for events which leave the residual

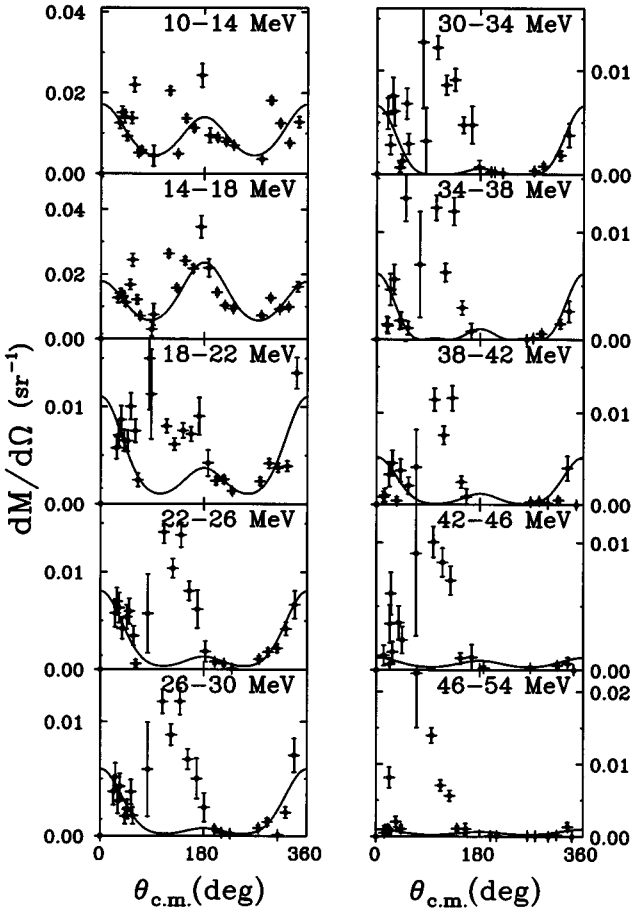

FIG. 12. Angular distributions of protons emitted in coincidence with ^{40}Ca fragments for events which leave the residual nucleus ^{39}K in the ground state, and for different excitation energy bins. Data are displayed in the rest frame of the excited ^{40}Ca recoil nucleus. Solid lines are a fit to the data (see text)

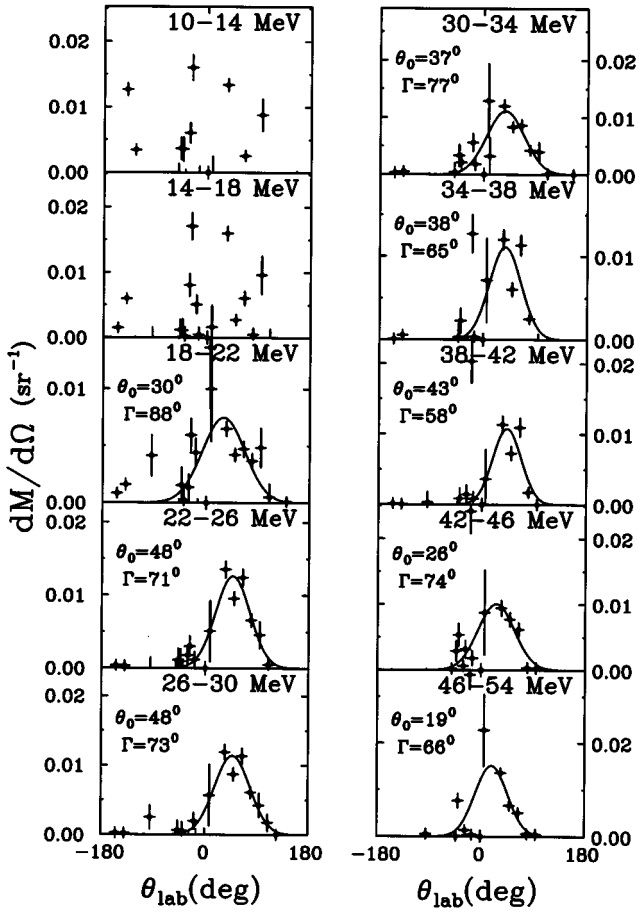

FIG. 13. Angular correlations in the laboratory frame after subtraction of the fits (see Fig. 12). The solid lines are a Gaussian fit to the data. θ_0 and Γ are the centroid and width (FWHM) of the Gaussian.

nucleus ^{39}K in the ground state. Data are displayed in the rest frame of the excited ^{40}Ca recoil nucleus for several excitation energy bins. $\theta_{\text{c.m.}}$ is the emission angle of the protons with respect to the direction of the recoil nucleus, increasing in the clockwise direction. A fit was performed using a polynomial up to the fourth power of the function cosine. Parameters were adjusted to fit only the backward detectors (with respect to the beam) where no process other than the emission by the recoil nucleus is expected. Under the assumption of the emission by the ^{40}Ca recoil nucleus, the data should exhibit a symmetric behavior around the recoil direction (θ=0°). However, a large deviation from the polynomial fit is observed between 90° and 180°, for all energy bins above 18 MeV, revealing the existence of another process for which the rest frame of the recoil nucleus is not the relevant system of reference. In order to get more quantitative information regarding this unexplained process, angular correlations were plotted in the laboratory frame after subtraction of the polynomial fits (Fig. 13). A Gaussian fit was performed for each of the bins which characteristics are displayed in the panels. In the last two bins the pick-up break-up mechanism starts to contribute which moves the excess yield to smaller angles. Excluding these last two bins, the average position and width [full width at half maximum (FWHM)] for our new component are 41° and 74°, respectively. Moreover, an asymmetry between 0° and 180° is clearly apparent in the fit for excitation energies between 18 and 38 MeV which is consistent with the presence of proton knockout by the projectile.

C. Fast proton emission

A useful concept for the analysis of the coincidence data is that of missing energy E_{miss}, which is defined as the excitation energy E^* minus the kinetic energy of the emitted light particle $E_p^{\text{c.m.}}$ and the kinetic energy of the target remnant $E_{T'}$ in the center of mass of the recoiling target. $E_{\text{miss}}=E^*-E_p^{\text{c.m.}}-E_{T'}$. In the case of the emission of only one particle, E_{miss} is directly related to the final state energy of the daughter nucleus E_{fs} by $E_{\text{miss}}=E_{fs}-Q$, where Q is the binding energy of the emitted particle.

The contribution of the new component to the missing energy spectrum is shown in Fig. 14(a). Only excitation energies above 30 MeV have been included, and two groups of detectors have been selected, one around +50° [Fig. 14(a)], where the unexpected proton yield is observed, and the other at backward angles in the laboratory frame [Fig. 14(b)], where protons are coming from the target decay. For the two

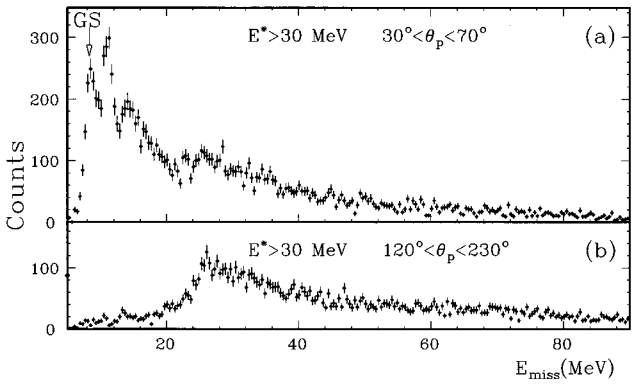

FIG. 14. Missing energy spectra displayed for two groups of detectors, one around +50° (a) and the other at backward angles in the laboratory frame (b), for excitation energies above 30 MeV.

spectra we observe a large bump around 30 MeV that corresponds to the decay of the target. For forward proton angles only (top of figure), an important contribution populating the GS and several excited states of the daughter nucleus ^{39}K is observed.

To extract the contribution to the inelastic spectrum of this new mechanism, the inelastic spectrum in coincidence with backward detectors ($120° \leqslant \theta_p \leqslant 160°$), where only target decay is present, was subtracted from the spectrum in coincidence with forward detectors ($30° \leqslant \theta_p \leqslant 70°$), after suitable normalization for the solid angles of the particle detectors. The two inelastic spectra, and the result of the subtraction are shown on Fig. 15, both with (right panel) and without (left panel) gating on discrete final states in ^{39}K ($E_{fs} < 8$ MeV). The two resulting spectra [Figs. 15(e) and 15(f)] are very similar, confirming that the fast mechanism mainly populates the low-lying states of ^{39}K. The contribution of this mechanism to the inelastic spectrum sets in at around 20 MeV excitation energy and therefore does not contribute to the inelastic cross section in the GR region. Its maximum is located around 30 MeV. Above, this contribution decreases but persists up to excitation energies as high as 80 MeV. In order to extract quantitatively the contribution of this mechanism to the inclusive inelastic spectrum, knowledge of the out-of-plane correlation between the ejectile and the proton would be necessary. Similar observations have been made in the inelastic reactions ^{208}Pb(^{17}O, ^{17}O n) [31], ^{90,94}Zr(^{36}Ar, ^{36}Ar n) [32], and ^{58}Ni(^{40}Ar, ^{40}Ar n or p) [33,34], where fast neutrons and protons emitted in the forward direction were observed. This latter experiment will allow us to bring new information such as the azimuthal angular correlation between the particle and the ejectile and the contribution of this new mechanism to the inelastic spectrum [35].

V. COINCIDENCE DATA: DECAY OF GIANT RESONANCES AND MULTIPHONON STATES

As quoted in the introduction of Sec. IV, the origin of the protons emitted at backward angles is emission from excited target states. In this section, an original method to sign multiphonon excitations in the inelastic spectrum through their

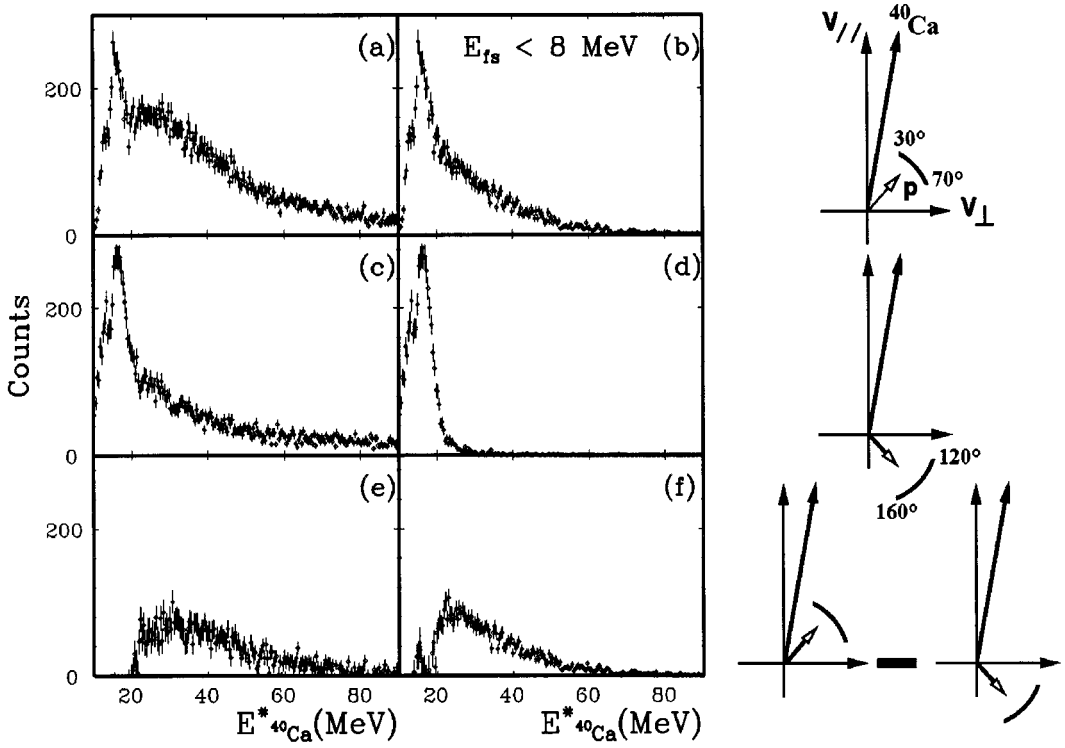

FIG. 15. Inelastic spectra in coincidence with protons emitted in the forward (a), (b) and backward (c), (d) directions and subtraction of the two spectra (e), (f) which shows the contribution of the new fast proton mechanism. Left panel (a), (c), (e) is for all events and right panel (b), (d), (f) for final state energies below 8 MeV in ^{39}K.

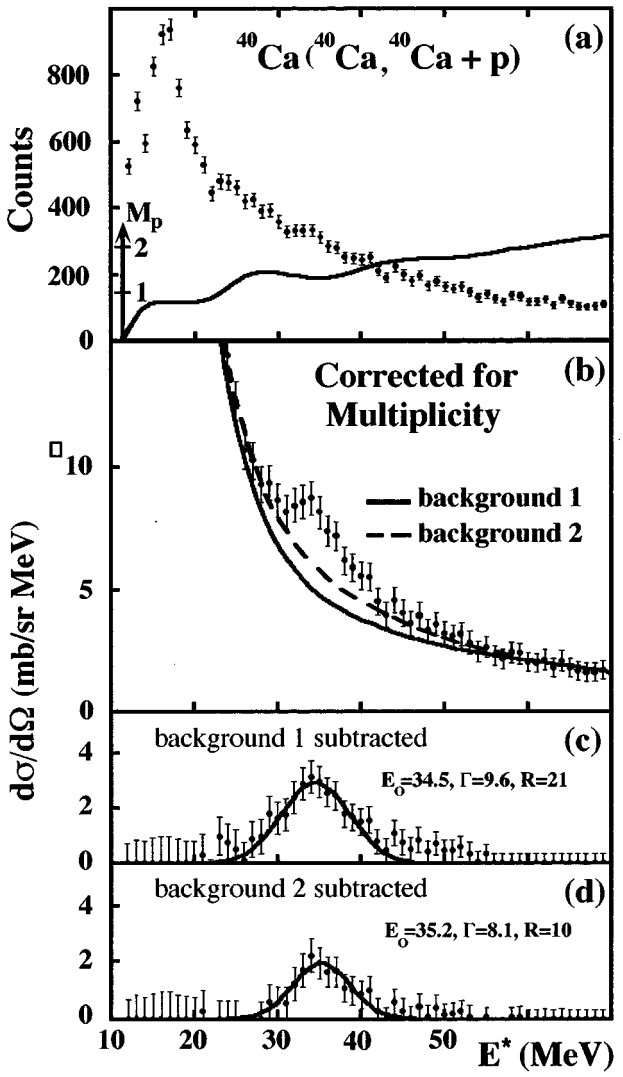

FIG. 16. (a) ^{40}Ca inelastic spectrum in coincidence with backward emitted protons. The proton multiplicity function calculated with LILITA is shown as a histogram. (b) Corrected spectrum with two estimated backgrounds shown as solid and dashed lines. (c), (d) Result of the subtraction of the backgrounds from the spectrum. Solid lines are Gaussian fits. E_0 and Γ are the centroid and the width (FHWM) of the Gaussian. R is the cross section ratio between the GR and the extracted bump.

specific particle decay pattern will be described. The exclusive inelastic spectra will be presented and the decay of the GR and higher excitation energy regions studied.

A. Inelastic spectrum in coincidence with backward emitted protons

The ^{40}Ca inelastic spectrum in coincidence with backward emitted protons is shown in Fig. 16(a). One should note that this spectrum has to be corrected for proton multiplicity with the excitation energy since events with larger multiplicity are detected with a greater efficiency [15]. Because of the small solid angle of our detection system, the probability to detect at least one proton is directly proportional to the multiplicity of emitted protons. The proton multiplicity as a function of excitation energy was calculated by two statistical decay codes LILITA and CASCADE. The result is very similar for the two codes and the multiplicity function calculated with LILITA is shown in Fig. 16(a) as a full line. The corrected spectrum, which is the coincidence spectrum divided by this multiplicity function, is displayed in Fig. 16(b). One should be aware that, in such a correction, the main assumption is that particle emission is purely statistical and a possible contribution of direct decay is not taken into account. However, in our case, the proton multiplicity of the direct decay of a multiphonon state built with a GR of energy around 16 MeV is similar to the multiplicity of a statistical decay from an equivalent energy region. In this regard we can consider that our multiplicity function deduced from the statistical codes reflects fairly well the target decay multiplicity.

The corrected coincidence spectrum [Fig. 16(b)], shows a prominent structure at twice the GQR excitation energy, which was barely visible in the inclusive spectrum (Fig. 5). In order to estimate the characteristics of this structure, several polynomial fits of the background were subtracted. Two examples of backgrounds are shown as solid and dashed lines in Fig. 16(b), and the result of their subtraction from the spectrum, fitted by Gaussians, are displayed in Figs. 16(c) and 16(d). From these two subtracted spectra, the energy of the structure is found to be 34.8 ± 0.5 MeV, the FWHM 8.8 ± 2 MeV, and the cross section 15 ± 8 times smaller than the giant resonance cross section. These characteristics are compatible with the multiphonon model [36] which predicts a two-phonon state at twice the energy of the GR, a width equal to $\sqrt{2}$ times the width of the one-phonon state and a cross section ratio of about 20 between the GR and the double phonon [37]. However, theoretical calculations for this energy region predict the presence of both the two-phonon state and other high-lying giant resonances [16]. Although, the structure observed appears to be a good candidate for a double quadrupole phonon excitation, a detailed study of its decay and a comparison with the direct decay pattern of the GQR is needed to confirm this hypothesis.

Indeed, as a giant resonance is understood as the first oscillator quantum, multiphonons can be defined as the higher quanta. A multiphonon excitation can be interpreted as a simultaneous excitation of n identical phonons, in other words, a giant resonance built on other GRs. In the picture where all phonons are excited and decay independently, each phonon is expected to exhibit the same direct decay properties as the giant resonance. The decay of the first phonon will populate the hole states of the daughter nucleus coupled to the remaining phonon which will then decay, feeding the two-hole states of the final nucleus. Therefore, the analysis of the decay of both the GR and the observed states at high excitation energies should allow us to characterize the presence of multiphonon strength.

B. Giant resonance decay

Particle decay of GRs can occur through various processes. The coupling of the particle-hole $(1p\text{-}1h)$ states to the continuum gives rise to the direct decay which populates the hole states of the A-1 residual nucleus with an escape width $\Gamma^{\uparrow}$. The study of such direct decay provides informa-

tion on the microscopic structure of the GR and can furnish a signature of a multiphonon state as will be shown in the following paragraph. The mixing of the $1p$-$1h$ states with more complicated states $2p$-$2h$, which can then couple again to $3p$-$3h$ and eventually to np-nh states until a completely equilibrated system is reached, leads to the statistical decay of the compound nucleus. This process, gives rise to the spreading width $\Gamma^{\downarrow}$. The statistical decay can be calculated by means of the Hauser-Feschbach formalism. In this case, no information on the microscopic structure of the initial state is conserved.

Experimentally, the direct decay part of the GQR is extracted by constructing the missing energy spectrum and by comparing it with the equivalent spectrum calculated with the statistical decay code CASCADE. For a given energy region, we calculate the proton energy spectrum for each 1 MeV wide bin with CASCADE, convolute it with a 800 keV Gaussian to simulate the experimental resolution, and transform it into missing energy spectrum by subtracting the proton energies from the excitation energy of the bin. Then we sum the results obtained for each bin with a weight given by the inclusive spectrum. Figure 17(a) compares the statistical calculation (histograms) to the data, for the GQR region ($12 \leqslant E^* \leqslant 20$ MeV). The calculation has been normalized so as to never overshoot the data, in order to obtain the maximum contribution consistent with statistical decay. An excess of cross section for decay to the GS, and the first excited hole state at 2.6 MeV of ^{39}K is observed, making up about 30% of the proton decay. This excess can be ascribed to direct decay, 16% populating the GS and 14% the first excited state. However, it must be recalled that a threshold of 4 MeV was set on the proton energy. One way to estimate the effect of the threshold is to assume that all protons of energy below 4 MeV are due to statistical decay. The fraction of protons below 4 MeV can then be calculated by the code CASCADE, and is found to be equal to 30% of the total number of protons emitted by statistical decay. Adding these low energy protons, which were not detected, to the measured number of statistically emitted protons, one obtains a 23% direct decay branch for the GQR region in ^{40}Ca. Yet it should not be forgotten that the GQR is superimposed over a background that was not identified but is due neither to the pickup breakup mechanism nor to the newly observed mechanism presented in Sec. IV C since their contribution sets in at a higher excitation energy. Our measurement includes the contribution from the background which induces a large uncertainty on the direct decay branch of the GQR. For example, if one assumes that this background is due to target excitation and that it decays purely statistically, the GQR direct decay branch would be 46%.

At least two previous measurements of the decay of the GQR in ^{40}Ca exist [38,39]. No statistical calculation were performed in these references and therefore the percentage of direct decay could not be extracted. However, the relative population of the GS (p_0 decay) and the first excited state (p_1 decay) were extracted for the energy region between 16.4 and 20.7 MeV in Ref. [39] and the two bumps of the GQR, 13.5 to 15.6 MeV and 15.6 to 22.5 MeV in Ref. [38]. In the region of the second bump these two measurements do not agree, Ref. [38] finds twice as much p_0 than p_1 whereas

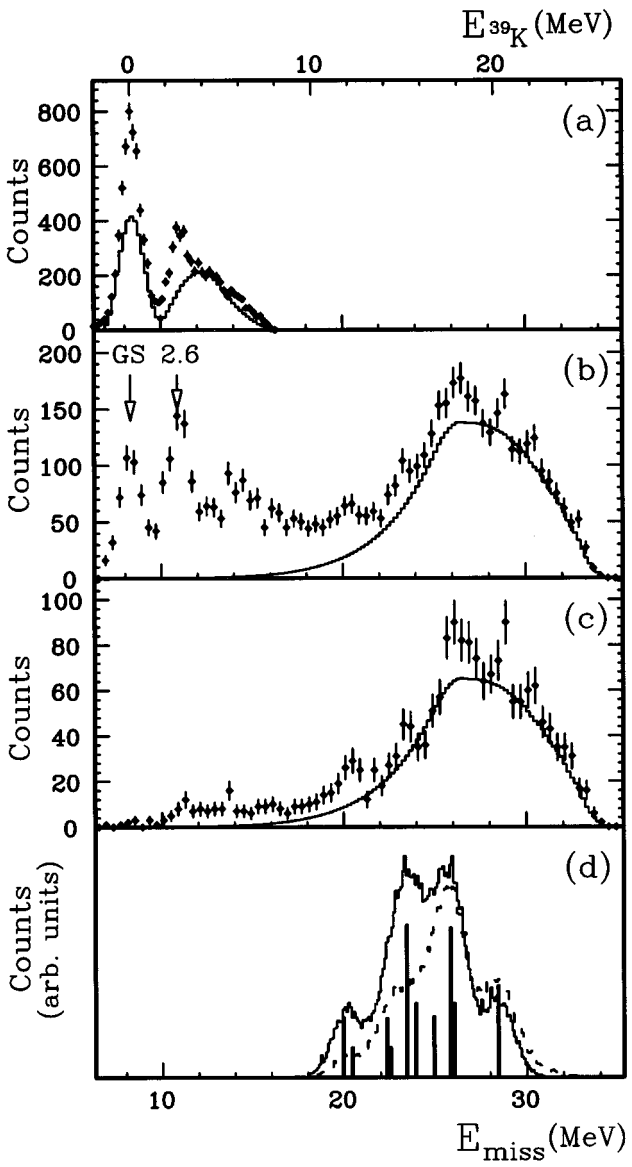

FIG. 17. (a) Missing energy spectrum gated on the GQR (12–20 MeV) for protons emitted in the backward direction between +50° and +250°. The histogram is the result of the CASCADE calculation (see text). (b) Same for the double phonon region (30–38 MeV). (c) same as (b) for detectors located between +120° and +235°. (d) Simulated missing energy spectrum for the double phonon direct decay. Solid line is for 100% direct decay and dashed line for 30% direct decay (see text). Vertical bars indicate the missing energy corresponding to the various decay paths. The upper scale shows the ^{39}K excitation energy.

Ref. [39] finds 3 times less p_0 than p_1. This could be due to very different proton energy thresholds in both experiments, 2 MeV in Ref. [39] and 4.6 MeV in Ref. [38]. In our work we find a ratio p_0 over p_1 of 0.9 for this energy region (15.6 to 22.5 MeV) in between the two measurements cited above with a proton threshold of 4 MeV. However, we should note that the background underlying the GQR is very different in light-ion or heavy-ion experiments making the comparison somewhat hazardous.

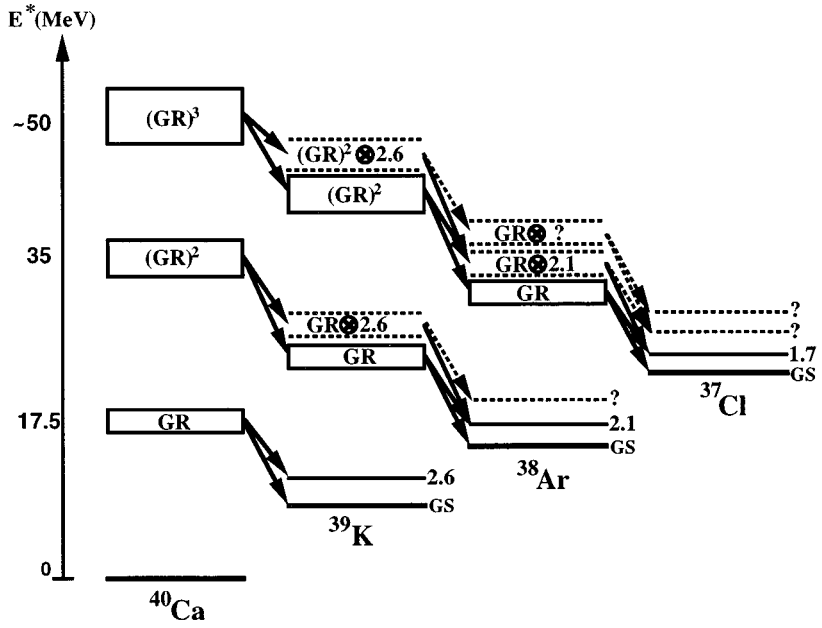

FIG. 18. Schematic diagram of the proton direct decay of the GR, the double and the triple phonon. The full arrows are the decays taken into account in the direct decay simulations while the dashed arrows are other possible decays.

C. Decay of the two-phonon state

For excitation energies in ^{40}Ca around 34 MeV, corresponding to the structure observed in Fig. 16, the missing energy spectrum [Fig. 17(b)] shows two main features. First of all, a population of the GS and the 2.6 MeV state in ^{39}K is observed. The angular correlations presented in Sec. IV B show that this component does not correspond to the direct decay of a GR but is due to a new dynamical effect. As shown in Fig. 17(c), this contribution completely disappears when restricting the coincidence to backward detectors located between $+120°$ and $+235°$ in the laboratory.

More surprisingly, various peaks located around 26 MeV missing energy show up, superimposed on a broad contribution. At these high excitation energies in ^{40}Ca, two protons can be emitted, while only one is detected. If the first proton is detected, peaks in the missing energy spectrum mean that a small number of states must be preferentially populated in ^{39}K around 17 MeV excitation energy. In the same way, if we detect the second emitted proton which populates the ^{38}Ar, peaks will show up only if the initial excited nucleus, ^{40}Ca, has decayed through particular states in ^{39}K, to well defined low lying states in ^{38}Ar. This is precisely the picture expected for the direct decay of a two-phonon state. For a statistical decay, no structure is expected in the missing energy spectrum. This is shown by the CASCADE calculation performed for this energy region which predicts a broad bump without any structure, centered around 28 MeV in the missing energy spectrum (histogram). In both spectra [Figs. 17(b) and 17(c)] an excess of cross section is observed centered at 26 MeV.

Figure 18 sketches the direct decay scheme of GRs as well as the proton direct decay of a double and a triple GR in ^{40}Ca. For the single phonon (GR), the proton direct decay populates the GS and the first hole states at 2.6 MeV of the ^{39}K. For a double GR two protons are emitted. The first emission will populate the hole states of the daughter nucleus coupled to the GR, and the second emission will feed the two-hole states of the final nucleus. A similar pattern would occur for the decay of the three-phonon state, feeding the three-hole states of the A-3 nucleus.

In order to ascertain if the peaks observed in the missing energy spectra are related to two-phonon excitations, a simulation of the direct decay of a double GR was performed with the following hypothesis. Both components of the GR (at 14 and 17.5 MeV) are assumed to populate by direct decay the GS and the first excited hole state at 2.6 MeV in ^{39}K with equal probability, using the information as extracted from the study of the GR decay. The GR built on the GS of ^{39}K can either populate the GS or the first excited two-hole state of ^{38}Ar at 2.1 MeV, while the GR built on the first excited one-hole state of ^{39}K can only decay to the excited two-hole states of ^{38}Ar, either the same 2.1 MeV state as mentioned above or a higher energy state. However, our present data does not provide enough information to know precisely which state is involved, and so our simulation will not include this last possible decay to a higher energy state. These different decay combinations taken into account give rise to well defined values of the missing energy. Due to the double bump of the single GR, ten values, shown by solid bars in Fig. 17(d), contribute to the missing energy spectrum. Taking into account the experimental resolution (800 keV) and a phonon width of 1.8 MeV for each the bump of the GR, the final result (histogram) exhibits a shape with four peaks in remarkable agreement with what is observed in the experimental missing energy spectrum. In this simulation we assume that whenever the first phonon has decayed directly, the second phonon has undergone a direct decay as well. However, if we take into account that the direct decay percentage is 30% for each of the phonons, we would expect that when the first phonon has decayed directly the second phonon has a 30% chance to decay directly and a 70% chance to decay statistically. The dot-dashed spectrum is obtained with this assumption, using CASCADE whenever the GR in ^{39}K decays statistically. In this case the peaks still persist but are less pronounced.

Another possible contribution to the missing energy spectrum built with one detected proton could come from the direct n-p decay channel. If we rely on the neutron to proton

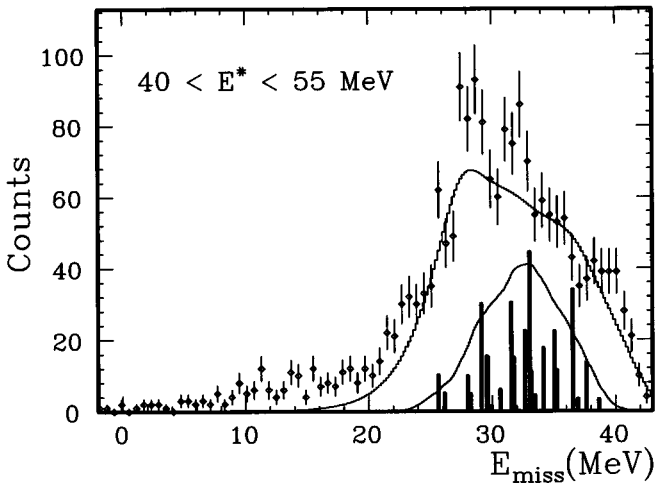

FIG. 19. Missing energy spectrum gated on the 40 to 55 MeV excitation energy region for the backward detector located between +120° and +235°. The histogram is the result of the CASCADE calculation while the solid line results from the simulation of the direct decay of a three-phonon state (see text). Vertical bars indicate the missing energy corresponding to the various decay paths.

ratio predicted for a purely statistical decay of the GR in ^{40}Ca, the double direct decay through a neutron first and then a proton should be small. Nevertheless, if such a case does occur, due to the high threshold for neutron emission, only the GS of ^{39}Ca would be populated, coupled to the second GR. Then, if we assume a proton direct decay to the GS of ^{38}K only, the corresponding missing energy would be 23.3 MeV, feeding the second lower peak observed in the data and also predicted by the proton-proton direct decay simulation. Therefore, the presence of such a decay channel would not alter the peaks predicted by the simulation, and was not taken into account. The comparison of the experimental missing energy spectrum that presents peaks around the excitation energy of the GR in ^{39}K and the direct-decay simulation that predicts such peaks for a direct decay of a two phonon state in ^{40}Ca conclusively demonstrates the existence of the double phonon built with the GQR in ^{40}Ca.

D. Higher excitation energy region

The method developed previously can be applied to search for higher order phonon strength. The missing energy spectrum for the backward detectors located between +120° and +235° is extracted for an excitation energy in ^{40}Ca of about 50 MeV (around the expected three-phonon excitation energy) and is shown in Fig. 19 together with the statistical decay calculation performed with CASCADE. The large bump around 30 MeV missing energy is rather well reproduced by this calculation although some excess strength is present. A tentative three phonon decay simulation has also been performed assuming a 100% proton direct decay branch feeding with equal probability the ground states of ^{39}K, ^{38}Ar, and ^{37}Cl, and their first excited hole states at 2.6, 2.1, and 1.7 MeV, respectively. Obviously other excited states, labeled with question marks in Fig. 18, ought to be included to take into account all the possible direct decays. Our present data however, with only one proton detected out of three emitted particles, does not provide enough information as to what other states are involved in the decay. Thus no definite conclusion can be draw from our data on the possible presence of a three-phonon state. In order to obtain more exclusive information and be able to sign the direct decay of a three-phonon state, one would have to detect all the decaying particles simultaneously.

VI. CONCLUSION

Inelastic scattering of ^{40}Ca on ^{40}Ca at 50 MeV/nucleon was studied in coincidence with protons measured over a large angular domain. An analysis of the inclusive inelastic spectrum shows that the giant resonance region is dominated by the excitation of the isoscalar GQR superimposed on a background. At higher excitation energies, several mechanisms contribute to the inelastic cross section. Particle coincidence measurements are demonstrated to be a powerful tool to disentangle these contributions.

In a cone of 30° around the beam direction, the proton cross section is dominated by fast protons emitted from pickup breakup reactions. This mechanism accounts for at most 30% of the inclusive inelastic cross section at apparent excitation energies above 30 MeV. Evidence for a proton knockout process is seen at angles around the recoil direction and for apparent excitation energies between 18 and 42 MeV.

Centered around +40°, a component of fast moving protons is observed, which strongly feeds the GS and the first excited states of ^{39}K. However, the angular distribution of this component is consistent neither with the direct decay of high-energy giant resonances, nor with pickup breakup reactions. The production mechanism of these protons remains for the moment an open question which should be addressed by dedicated experiments in order to enhance our knowledge of the rich phenomenology of very peripheral heavy ion encounters.

The investigation of target excitations with no contribution from other mechanisms is made possible by gating on backward emitted protons. The GQR region in ^{40}Ca was found to have a 23% direct decay branch towards the ground state and first excited state in ^{39}K. Furthermore, through the observation of its specific direct decay pattern, the presence of the double GQR has been demonstrated in the excitation energy region between 30 and 38 MeV. The energy (34.8 ± 0.5 MeV) and width (8.8 ± 2 MeV) of this state are in agreement with a harmonic picture of collective nuclear excitations. The cross section ratio between the one-phonon state (the GR) and the two-phonon state found to be 15 ± 8 is consistent with theoretical calculations [37]. Heavy-ion inelastic scattering at incident energy around 50 MeV/nucleon, combined with particle decay measurement is thus a unique tool to investigate multiphonon states built with the giant quadrupole resonance in nuclei. Recently, the two-phonon GDR was observed in various nuclei with different experimental probes: pion double charge exchange reactions at LAMPF (Los Alamos) [40,41], and relativistic heavy-ion Coulomb excitation at SIS (Darmstadt) [42–44].

Up to now, the existence of the two phonon GQR and the two phonon GDR has been clearly established. No solid evi-

dence of triple phonon states has been found to date. The most promising path towards the observation of the triple GQR is the particle decay method presented here. However, the present experimental setup, with a particle detection efficiency of less than 3%, cannot meet the challenge. A straightforward way to increase this efficiency would be the use of a 4π charged particle array in coincidence with a spectrometer. This would also allow to detect simultaneously all particles emitted by a multiphonon state, leading to a more precise understanding of its decay.

ACKNOWLEDGMENTS

We wish to thank P. Gangnant, L. Garreau, and J.F. Libin for their technical help during the experiment. This experiment was performed at the GANIL national facility, Caen, France.

[1] N. Frascaria, C. Stephan, P. Colombani, J.P. Garron, J.C. Jacmart, M. Riou, and L. Tassan-Got, Phys. Rev. Lett. **39**, 918 (1977).
[2] N. Frascaria *et al.*, Z. Phys. A **294**, 167 (1980).
[3] Ph. Chomaz *et al.*, Z. Phys. A **319**, 167 (1984).
[4] N. Frascaria, Y. Blumenfeld, Ph. Chomaz, J.P. Garron, J.C. Jacmart, J.C. Roynette, T. Suomijärvi, and W. Mittig, Nucl. Phys. **A474**, 253 (1987).
[5] N. Frascaria, Nucl. Phys. **A482**, 245c (1988).
[6] T. Suomijärvi *et al.*, Nucl. Phys. **A509**, 369 (1990).
[7] R. Liguori-Neto *et al.*, Nucl. Phys. **A560**, 733 (1993).
[8] Y. Blumenfeld, J.C. Roynette, Ph. Chomaz, N. Frascaria, J.P. Garron, and J.C. Jacmart, Nucl. Phys. **A445**, 151 (1985).
[9] A. van der Woude, Prog. Part. Nucl. Phys. **18**, 217 (1987).
[10] J.A. Scarpaci *et al.*, Phys. Lett. B **258**, 279 (1991).
[11] J.A. Scarpaci *et al.*, Phys. Rev. Lett. **71**, 3766 (1993).
[12] H. Emling, Prog. Part. Nucl. Phys. **33**, 729 (1994).
[13] Ph. Chomaz and N. Frascaria, Phys. Rep. **252**, 275 (1995).
[14] L. Bianchi *et al.*, Nucl. Instrum. Methods Phys. Res. A **276**, 509 (1989).
[15] J.A. Scarpaci, Ph.D. Thesis, Université d'Orsay, France, 1990.
[16] Y. Blumenfeld and Ph. Chomaz, Phys. Rev. C **38**, 2157 (1988).
[17] J. Raynal, Phys. Rev. C **23**, 2571 (1981).
[18] C.R. Gruhn, T.Y.T. Kuo, C.J. Maggiore, H. McManus, F. Petrovich, and B.M. Preedom, Phys. Rev. C **6**, 915 (1972).
[19] R. H. Spear, At. Data Nucl. Data Tables **42**, 91 (1989).
[20] J.R. Beene, D.J. Horen, and G.R. Satchler, Phys. Lett. B **344**, 67 (1995).
[21] T. Suomijärvi *et al.*, Nucl. Phys. **A491**, 314 (1989).
[22] V. Borrel, B. Gatty, D. Guerreau, J. Galin, and D. Jacquet, Z. Phys. A **324**, 205 (1986).
[23] K. Siwek-Wilczynska, J. Wilczynski, C.R. Albiston, Y. Chan, E. Chavez, S.B. Gazes, H.R. Schmidt, and R.G. Stokstad, Phys. Rev. C **35**, 1316 (1987).
[24] L. Tassan-Got (private communication).
[25] J. Gomez del Campo and R.G. Stokstad, Internal Report No. ORNL TM7295 (unpublished).
[26] J.C. Roynette, N. Frascaria, Y. Blumenfeld, J.C. Jacmart, E. Plagnol, J.P. Garron, A. Gamp, and H. Fuchs, Z. Phys. A **299**, 73 (1981).
[27] M.H. Macfarlane and S.C. Pieper, ANL Report No. ANL-76-11, 1976 (unpublished).
[28] F. Pühlhofer, Nucl. Phys. **A280**, 267 (1977).
[29] W. von Oertzen, Phys. Lett. **151B**, 95 (1985).
[30] F. Zwarts, A.G. Drentje, M.N. Harakeh, and A. van der Woude, Nucl. Phys. **A439**, 117 (1985).
[31] A.M. van den Berg *et al.*, Nucl. Phys. **A578**, 238 (1994).
[32] V. Pascalon, Ph.D. Thesis, Université d'Orsay, France, 1997.
[33] J.A. Scarpaci *et al.*, in *Proceedings of the 14th RCNP Osaka International Symposium*, edited by H. Ejiri, T. Noro, K. Takahisa, and H. Toki (World Scientific, Singapore, 1996), p. 312.
[34] J.A. Scarpaci *et al.*, Proceedings of the International Symposium on Large-Scale Collective Motion of Atomic Nuclei, Brolo, Italy, 1996 (unpublished).
[35] J.A. Scarpaci *et al.* (in preparation).
[36] Ph. Chomaz and N.V. Giai, Phys. Lett. B **282**, 13 (1992).
[37] F. Catara, Ph. Chomaz, and A. Vitturi, Nucl. Phys. **A471**, 661 (1987).
[38] A. Moalem, W. Benenson, G.M. Crawley, and T.L. Khoo, Phys. Lett. **61B**, 167 (1979).
[39] D.H. Youngblood, A.D. Basher, D.R. Brown, J.D. Bronson, J.M. Moss, and C.M. Rozsa, Phys. Rev. C **15**, 246 (1977).
[40] S. Mordechai *et al.*, Phys. Rev. Lett. **60**, 408 (1988).
[41] S. Mordechai and C. Fred Moore, Nature (London) **352**, 393 (1991).
[42] J. Ritman *et al.*, Phys. Rev. Lett. **70**, 533 (1993).
[43] R. Schmidt *et al.*, Phys. Rev. Lett. **70**, 1767 (1993).
[44] K. Boretzky *et al.*, Phys. Lett. B **384**, 30 (1996).